

Phase transitions in magnetic superlattices

R. E. Camley

Department of Physics, University of Colorado, Colorado Springs, Colorado 80933-7150

D. R. Tilley

Department of Physics, University of Essex, Wivenhoe Park, Colchester, CO4 3SQ, England

(Received 5 May 1987)

We investigate the magnetic-field- and temperature-dependent equilibrium structure of magnetic superlattices formed from two ferromagnetic materials which couple antiferromagnetically at the interfaces. Both a macroscopic, Landau-Ginzburg, and a microscopic approach are used. Due to competing exchange and Zeeman interactions, a variety of phases exist in the superlattice. There are aligned phases where all the spins are either parallel or antiparallel to the applied field, and there is a twisted phase where the spins in each layer lie at a different angle with respect to the applied field. We show that small changes in the layering structure can lead to dramatic changes in the phase diagram.

I. INTRODUCTION

One of the most important features of superlattices is that the properties of the superlattice may be tailored by varying the layering sequence. Magnetic superlattices, in particular, can be very sensitive to changes of even one layer. For example in a superlattice composed of ferromagnetic films alternating with antiferromagnetic films, the ground state of the system depends critically on the number of microscopic layers inside each antiferromagnetic film.¹ An odd number of layers is more likely to produce a ground state where the spins all line up either parallel or antiparallel to an applied magnetic field. In contrast, an even number of layers in the antiferromagnet often produces a twisted state where the individual spins are at some angle to the magnetic field. The differences in the ground state generally also produce differences in the spin-wave excitations which propagate through the superlattice. Such differences can then lead to variations in the ir absorption spectrum that can be tailored to be in a desired frequency range.

Many earlier papers on phase transitions in magnetic superlattices considered only the case $T=0$ and discussed phase transitions produced by an external field which varied in magnitude.^{1,2} There have also been some studies of temperature dependence in superlattices (calculations of the critical temperature as a function of the layering for example) using a Landau-Ginzburg expansion of the free energy.³ The thermodynamic studies have concentrated primarily on the case of two ferromagnets which are also coupled ferromagnetically at the interface. This system is particularly simple since the ground state always has all the spins pointing in the same direction, the direction of an applied magnetic field.

In this paper we will consider in detail a rather intriguing system—a superlattice composed of two different ferromagnets which couple antiferromagnetically at the interfaces. Such a superlattice might be formed from alter-

nating layers of Fe and Gd for example.^{4,5} We will examine the H - T phase diagram of this system using both a microscopic treatment as well as a Landau-Ginzburg expansion. In contrast to the superlattice composed of ferromagnetic layers which are ferromagnetically coupled, we will see that our system can have many different ground states and as a result have a variety of possible phase transitions. We would like to note that in addition to the Fe/Gd system, there are a number of other material combinations which might be reasonably treated as two ferromagnets with antiferromagnetic coupling present at the interfaces. The combination of a rare-earth and transition metal often leads to an antiparallel magnetic coupling between the rare-earth $4f$ and $5d$ spin moment and the $3d$ moment of the transition metal.⁴ In addition, we may consider the Fe/Cr/Fe system^{6,7} where a very thin Cr film causes antiferromagnetic coupling between the Fe films. Similar constructions include the Fe/Ag/Fe systems,⁸ and FeNi films separated by EuS.⁹ We expect our model system to provide a qualitative guide to the behavior to be expected for systems with antiferromagnetic coupling.

In our work, we consider a model system of a bcc ferromagnet with $S = \frac{5}{2}$ (Fe) which is coupled antiferromagnetically at the interfaces to another bcc ferromagnet with $S = \frac{7}{2}$ (Gd). Of course bulk Gd is not a bcc structure and the anisotropy fields in bulk Gd, which we neglect here, play an important role in a spin reorientation transition near $T = 234$ K.¹⁰ Nonetheless, our model should give the general properties of the superlattice correctly within the limitations of the mean-field approximation. We also include an external magnetic field along the z direction. We find that there are basically four possible ground state configurations in the low-temperature and low-field limit.

(1) All the Gd spins are aligned with the magnetic field and all the Fe spins are antiparallel to the applied field.

We call this state aligned Gd.

(2) All the Fe spins are aligned with the magnetic field and all the Gd spins are antiparallel to the applied field. We call this state aligned Fe.

(3) A state where both the Gd and Fe spins are at an angle with respect to the external field. The direction and magnitude of this angle varies with position. This is the twisted state.

(4) A state where some of the Gd spins behave paramagnetically while the Fe spins are still ordered ferromagnetically.

The various states come about because of competition between Zeeman energy, which would be minimized if all the spins would line up with the external field, and the exchange energy, which would be minimized if the Gd spins and the Fe spins were oppositely oriented. We will discuss the details of this competition in detail later. As we will see, which state is the ground state will depend critically on the number of layers of Fe and Gd as well as the temperature and the applied field. This will allow us to gain considerable flexibility in designing the properties of the superlattice.

The remainder of the paper is as follows. In Sec. II we consider the superlattice from the microscopic point of view and obtain the H - T phase diagram for a number of structures by numerically minimizing the free energy for the superlattice. In Sec. III we develop the Landau-Ginzburg expansion for the free energy, including the effect of sharp interfaces. We then apply this work to the case for low temperatures and find the ground states and spin configurations as a function of applied magnetic field. Finally in Sec. IV we present a short summary.

II. MICROSCOPIC APPROACH TO SUPERLATTICES

The geometry of the structure is illustrated schematically in Fig. 1. An applied field, H_0 , is directed along the z axis. There are n_1 layers of material 1 (Fe) and n_2 layers of material 2 (Gd) in each unit cell of the superlattice.

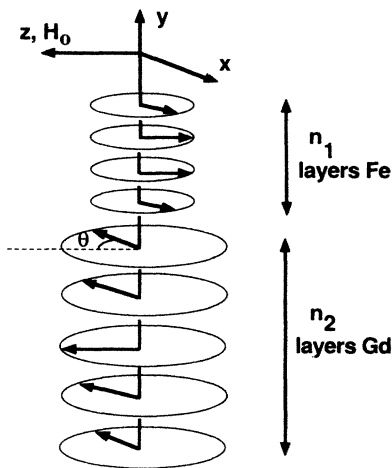


FIG. 1. Schematic illustration of the geometry of a unit cell of the superlattice. There are n_1 layers of Fe and n_2 layers of Gd. The spins in each layer may make different angles with respect to an applied field.

The Fe and Gd spins are free to rotate in the xz plane as shown in Fig. 1. (The spins are not likely to have static components in the y direction because this would set up static demagnetizing fields.)

In this work we consider nearest-neighbor interactions only. The inclusion of additional neighbors is straightforward. The exchange-coupling constant between Fe spins is J_1 , between Gd spins is J_2 , and between a Fe and a Gd spin is J_I . For this paper we take the case where both J_1 and J_I are fairly strong compared to J_2 . Our parameters have the values $J_1=1$, $J_I=-1$, and $J_1/J_2=0.155$. The ratio J_1/J_2 is obtained by comparing the transition temperature for Fe and Gd.

The method used to find the ground state of the superlattice structure at a given temperature and applied field has been described previously in a paper dealing with spin reorientations in thin Gd films on Fe substrates.¹¹ For completeness, however, we give a brief outline of this method here. It is best to start by finding the ground state at $T=0$. In this case the spin configuration of the superlattice is described by a set of n_1+n_2 angles which give the deviation of the spins in each plane of the unit cell.

The ground state is found by an iteration method. Once an initial configuration is chosen, we may find the effective field, H_i , which acts on the spin in layer i . This effective field is the sum of the exchange field and the external field. Thus for a bcc structure H_i is given by

$$H_i = 4(J_{i,i+1}S_{i+1} + J_{i,i-1}S_{i-1}) + H_0z. \quad (2.1)$$

Here $J_{i,i+1}$ is the exchange-coupling constant between spins in layers i and $i+1$, H_0 is the external field, and S_i is the spin in layer i . The iteration procedure now works as follows. We randomly pick a spin in a particular layer. The effective field acting on that spin is found through Eq. (1) and the spin is rotated to point in the direction of the effective field. This necessarily lowers the energy of the structure. A new spin in a different layer is then randomly chosen and rotated to lie along its effective field. This process is continued until one has a self-consistent state where all spins are aligned with the effective fields produced by the neighboring spins. Different initial configurations may lead to different self-consistent final states. The ground state is of course the lowest-energy final state which is also stable.

We have left out one point in the above discussion. The layers of spins at the ends of the unit cells will naturally be coupled to spins in other unit cells. One would normally expect that spins in equivalent layers in different unit cells would be related by a phase factor of the form $\exp(iqL)$. We have taken $q=0$ so that the equivalent layers of spins in all unit cells all point in the same direction. This is certainly the simplest and most likely case. An extension of the method to finite q is straightforward.

For finite T , both the direction and thermal averaged magnitude of the spins in each layer must be specified. In this case the iteration procedure operates as follows. A spin is first rotated into the direction of the effective field, and then its thermal averaged magnitude in that direc-

tion is found through the use of the Brillouin function

$$\langle S_i \rangle = S_i B_{S_i}(x), \quad (2.2)$$

where

$$x = \frac{S_i H_i}{kT} \quad (2.3)$$

and the Brillouin function is given by

$$B_s(x) = \frac{2S+1}{2S} \coth \left[\frac{(2S+1)x}{2S} \right] - \frac{1}{2S} \coth \left[\frac{x}{2S} \right]. \quad (2.4)$$

Here $\langle S_i \rangle$ is the thermal average of the spin in the i th layer in the direction of the effective field. The effective field H_i is still given by Eq. (2.1) but now the spins S_{i+1} and S_{i-1} are replaced by their thermal averages as well. Again the entire operation is repeated for all spins in a unit cell until a self-consistent state results.

Depending on the initial spin configuration, different final self-consistent states can be found. For finite T , one must choose a stable state with the lowest free energy. The free energy, as usual, is given by

$$F = -kT \ln(Z), \quad (2.5)$$

where Z is the partition function for the unit cell of the superlattice. In the mean-field approximation Z is given by

$$Z = \prod_i Z_i, \quad (2.6)$$

where Z_i is the partition function for the spin in layer i in the self-consistent effective field. Z_i is given simply by

$$Z_i = \frac{\sinh[(2S_i+1)H_i/2kT]}{\sinh[H_i/2kT]}. \quad (2.7)$$

The stability of the various phases is defined numerically. If we choose the initial configuration to be arbitrarily close to the configuration of interest and the iterative program diverges away from this configuration, then that structure is unstable.

The H - T phase diagram for the superlattice can now

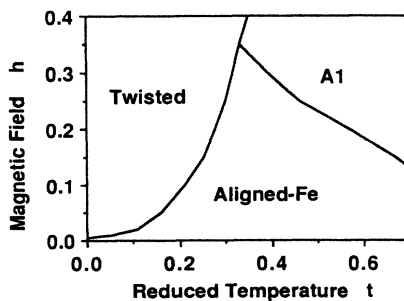


FIG. 2. Phase diagram for the superlattice with a unit cell of seven Fe layers and five Gd layers. The reduced temperature is T/T_c , where T_c refers to the transition temperature for bulk Fe. The field is given in dimensionless units by $h = H_0/JS_{Fe}$.

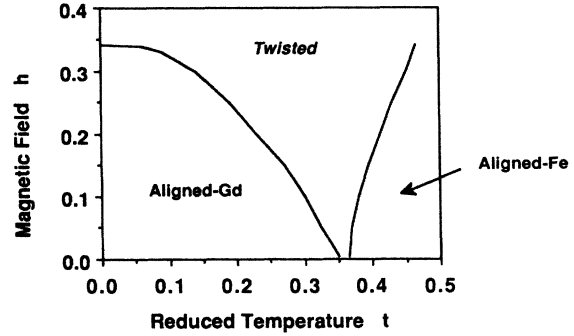


FIG. 3. Phase diagram for the superlattice with a unit cell of four Fe layers and four Gd layers. The reduced temperature is T/T_c , where T_c refers to the transition temperature for bulk Fe. The field is given in dimensionless units by $h = H_0/JS_{Fe}$. Notice that the transition between the aligned-Gd state and the twisted state takes place well above the transition temperature for bulk Gd of $t = 0.275$.

be determined by using the numerical method outlined above. As examples, we will consider two special cases: (1) The unit cell contains seven Fe spins and five Gd spins, and (2) the unit cell contains four Fe spins and four Gd spins. The phase diagrams for the two cases are presented in Figs. 2 and 3. As can be easily seen, the small change in the structure results in phase diagrams which are completely different.

We consider first case (1). For low temperatures and moderate fields, the ground state is a twisted state illustrated in Figs. 4(a) and 4(b). As the temperature is increased, the ground state becomes an aligned state [see Fig. 4(c)] where the Fe spins all point along the direction of the external field and all the Gd spins point opposite to the external field. As the temperature is further increased, we come to the state labeled A1, where the innermost layer of spins in the Gd film has become paramagnetic.

To understand the basic features of the phase diagram, we consider first the $T = 0$ situation. Here an aligned state, either aligned-Gd or aligned-Fe, has no net Zeeman energy. The aligned state is unstable, and the system

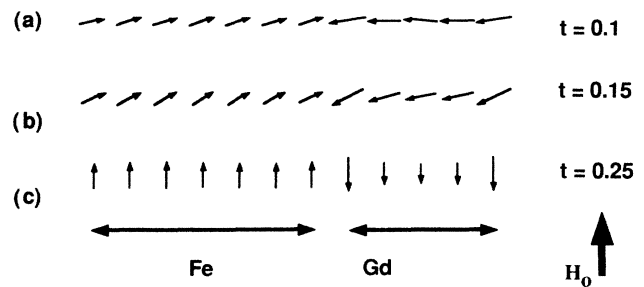


FIG. 4. Illustration of the spin positions for the various phases of the 7Fe/5Gd superlattice. All states are for $h = 0.1$. (a) and (b) are twisted states, while (c) is an aligned-Fe state. We show an entire unit cell of the superlattice with seven layers of Fe and five layers of Gd. The thermal average values for the magnitude of the spins are proportional to the length of the arrows representing the spin in each layer.

flops into a configuration where both the Gd and Fe spins are nearly perpendicular to the field but have small components parallel to the field. This is the twisted state of the superlattice. (This situation is analogous to the spin-flop state in antiferromagnets.)

The actual configuration in the twisted state depends on the competition between the exchange energy, which would be minimized if all Gd were all antiparallel to all Fe spins, and the Zeeman energy, which would be minimized if all the spins pointed along the external magnetic field. Such a situation is very similar to the competition between the exchange energy and the anisotropy energy which leads to domain walls. In fact, the twisted state discussed here is very reminiscent of the structure found in a domain wall as can be seen in Fig. 4. In domain walls, an increase in the anisotropy energy, which gives a preferred direction for the spins, results in a decrease in the width of the domain wall. Here an increase in the magnetic field, which again gives a preferred direction for the spins, results in a decrease in the width over which there is significant rotation of the spins. This is easily seen in Fig. 5 where we plot twist angle as a function of position for different magnetic fields.

As the temperature is increased, the thermal averaged magnetic moment of the Gd spins decreases rapidly compared to the thermal averaged magnetic moment of the Fe spins (the exchange constant for Gd-Gd interactions is much smaller than that for Fe-Fe interactions). As a result, the amount of Zeeman energy which can be gained from the Gd spins is reduced. The competition between the Zeeman and exchange energies now forces the Fe and Gd spins to become progressively more antiparallel and also the Fe spins begin to point closer to the direction of the applied field. As the temperature is further increased, we get a smooth second-order phase transition to the aligned state where all Fe point along the external field and all the Gd point opposite to the external field.

The behavior of the different layers of spins as a function of temperature in the aligned state is also interesting. The outermost Gd spins see a large effective exchange field due to the strong coupling of the neighboring Fe spins. As the temperature is increased, the thermal averaged magnetic moment of these spins decreases slowly. In contrast, the inner Gd spins see a smaller effective field

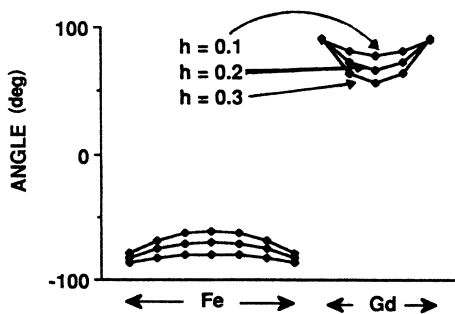


FIG. 5. Twist angle as a function of position for different applied fields for a 7Fe/5Gd superlattice. We show an entire unit cell of the superlattice with seven layers of Fe and five layers of Gd.

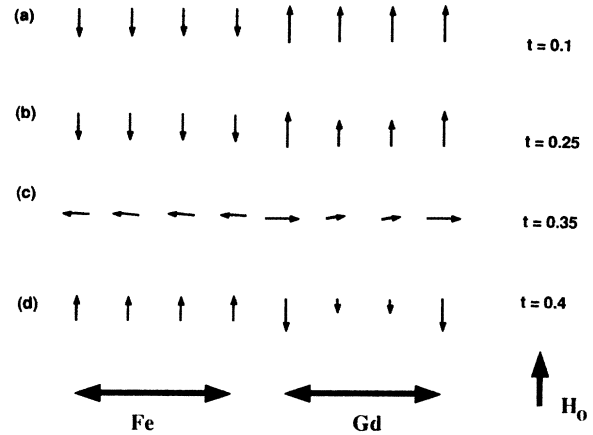


FIG. 6. Illustration of the spin configuration for the various phases of the 4Fe/4Gd superlattice. All states are for $h = 0.01$. (a) and (b) show the aligned-Gd state at two different temperatures, (c) is the twisted state, and (d) is the aligned-Fe state. The figures show a unit cell of the superlattice with four layers of Fe and four layers of Gd.

and thus develop a smaller thermal averaged moment. This leads to the structure seen in Fig. 4(c), where the inner Gd spins have a significantly smaller moment than the outer Gd spins. As the temperature is further increased, the innermost Gd spin eventually undergoes a transition to paramagnetic behavior. This spin then lines up with the external field, and the system is in the A1 state.

The superlattice with four Gd layers and four Fe layers in a unit cell has qualitatively different behavior. In this case at $T = 0$ the Zeeman energy of the system is lower for the aligned state with Gd parallel to the field (and Fe antiparallel) than for the aligned state with Fe parallel to the field (and Gd antiparallel). The aligned-Gd state is also stable and is thus the ground state. As the temperature is increased, the average Gd moment is reduced and eventually the Zeeman energy of the Gd spins and the Fe spins sum to zero. Here, as in the case of seven Fe layers and five Gd layers, the aligned state becomes unstable, and the system flops into the twisted state. As the temperature is further increased, there is another transition into the aligned-Fe state where the Fe spins point along

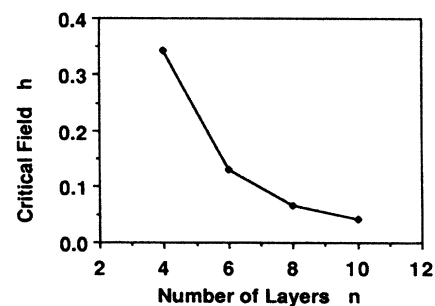


FIG. 7. Critical field for the transition from the aligned-Gd state to the twisted state at $T = 0$ as a function of number of layers n in an $n\text{Fe}/n\text{Gd}$ superlattice.

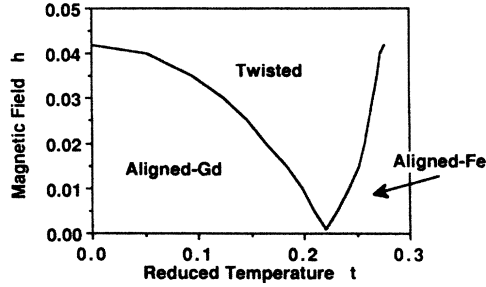


FIG. 8. Phase diagram for the superlattice with a unit cell of ten Fe layers and ten Gd layers. Here in contrast to Fig. 3 the transition between the aligned-Gd state and the twisted state takes place below the transition temperature of bulk Gd.

the field and the Gd spins are antiparallel to the field. This transition from the twisted state to the aligned-Fe state occurs for the same reasons as it does in the system with unit cell 7Fe/5Gd. The spin configurations in the different phases are shown in Fig. 6.

The transition between the twisted and aligned-Gd state at $T=0$ for the 4Fe/4Gd superlattice occurs at a very high field. This field depends critically on the number of layers in each ferromagnetic film. In Fig. 7 we plot the critical field as a function of number of layers n for an n Fe/ n Gd superlattice. We see in this figure that as n is increased, there is a dramatic reduction of the field required to cause a transition from the aligned-Gd to the twisted state, a result similar to one found in ferromagnetic-antiferromagnetic superlattices.¹ In an earlier paper,¹¹ we argued that the twisted state was to be expected whenever the penetration depth of the twist was smaller than the numbers of layers in the film. Since the penetration depth of the twist increases as H is decreased, a larger film will allow twisted states at smaller applied fields. As an example, the phase diagram for a superlattice with a unit cell of 10Fe/10Gd is presented in Fig. 8. This phase diagram looks very similar to the one for a superlattice with unit cell 4Fe/4Gd except that the magnetic field has been reduced by about a factor of 10. Note also that the transition temperature between the aligned and the twisted states for $H=0$ has been reduced.

We have seen in this section that microscopic changes in the layering pattern lead to significant differences in the ground-state configurations. There will, of course, be macroscopic consequences as well. Clearly, the spin-wave excitation spectrum will be different for different ground states. In addition the magnetization and magnetic susceptibility will also depend on the ground state.

III. CONTINUUM APPROXIMATION

A. General formulation

When the change in spin value and orientation from one site to the next within either medium is not too great, the microscopic mean-field theory used in the preceding section can be approximated by a continuum theory. This has the advantages that explicit analytic expressions can be given for the twisted states, and that these expres-

sions apply for all values of the thickness of the two media.

The continuum theory can be derived by a Taylor-series expansion of the free-energy expression resulting from the Hamiltonian; an explicit example is given by Cottam *et al.*¹² It is more straightforward in the present case simply to write down the free energy in terms of the invariants of the system. Let \mathbf{M} be the vector representing a spatially varying magnetization in a film occupying the space $-d_1 < y < 0$. Similarly \mathbf{N} is the magnetization in the region $0 < y < d_2$. We restrict attention to twisted states, in which reconstruction consists of rotations about the y axis so that the magnetizations \mathbf{M} and \mathbf{N} have components (M_x, M_z) and (N_x, N_z) . Within medium 1, the free energy is expanded in terms of the second- and fourth-order invariants under rotation about the y axis:

$$F_1 = \int_{-\infty}^{\infty} dx dz \int_{-d_1}^0 dy \left\{ -B_0 M_z + \frac{1}{2} a_1 (M_x^2 + M_z^2) + \frac{1}{4} b_1 (M_x^2 + M_z^2)^2 + \frac{1}{2} c_1 [(\nabla M_x)^2 + (\nabla M_z)^2] \right\}. \quad (3.1)$$

The parameter c_1 determines the characteristic length for changes in \mathbf{M} . For the Heisenberg Hamiltonian on a bcc lattice, the corresponding term in the Taylor expansion is

$$(3J_1/d) \int dx dy dz [(\nabla S_x)^2 + (\nabla S_z)^2], \quad (3.2)$$

where d is the cube edge. Comparison of the terms with the use of the usual relation

$$\mathbf{M} = g\mu_B \mathbf{S} / \Omega, \quad (3.3)$$

where $\Omega = d^3/3$ is the volume per spin gives

$$c_1 = 3J_1 d^5 / 4g^2 \mu_B^2. \quad (3.4)$$

This determines the characteristic length in terms of microscopic parameters.

The free energy in medium 2, F_2 , is given in terms of \mathbf{N} by the same expression as F_1 , with parameters a_2, b_2, c_2 . The presence of the interface at $y=0$ introduces the additional invariants $(M_x^2 + M_z^2)_{y=0}$, $(N_x^2 + N_z^2)_{y=0}$, and $(M_x N_x + M_z N_z)_{y=0}$, so that the interface free energy is

$$F_{I0} = \int_{-\infty}^{\infty} dx dz \left\{ \frac{1}{2} c_1 \delta_1^{-1} (M_x^2 + M_z^2)_0 + \frac{1}{2} c_2 \delta_2^{-1} (N_x^2 + N_z^2)_0 + \alpha (M_x N_x + M_z N_z)_0 \right\}. \quad (3.5)$$

The final term expresses the coupling across the interface. Comparison with the expression

$$-\frac{1}{2} (J_1/d^2) \int_{-\infty}^{\infty} dx dz (S_{1x} S_{2x} + S_{1z} S_{2z}) \quad (3.6)$$

derived from the Hamiltonian gives α in terms of the exchange parameter J_1 . For our model of gadolinium on iron, J_1 is antiferromagnetic and α is positive.

The equilibrium configuration is found from the Euler-Lagrange equations for the minimum value of the total free energy $F = F_1 + F_2 + F_I$, namely

$$-\mathbf{B}_0 + a_1 \mathbf{M} + b_1 |\mathbf{M}|^2 \mathbf{M} - c_1 \frac{\partial^2 \mathbf{M}}{\partial y^2} = 0, \quad (3.7)$$

$$-\mathbf{B}_0 + a_2 \mathbf{N} + b_2 |\mathbf{N}|^2 \mathbf{N} - c_2 \frac{\partial^2 \mathbf{N}}{\partial y^2} = 0, \quad (3.8)$$

with boundary conditions at $y=0$.

$$c_1 \left[\frac{\partial \mathbf{M}}{\partial y} + \delta_1^{-1} \mathbf{M} \right] + \alpha \mathbf{N} = 0, \quad (3.9)$$

$$c_2 \left[\frac{-\partial \mathbf{N}}{\partial y} + \delta_2^{-1} \mathbf{N} \right] + \alpha \mathbf{M} = 0. \quad (3.10)$$

B. Constant-amplitude approximation

The full set of Eqs. (3.7)–(3.10) is quite formidable, and we, therefore, reduce them by means of the constant-amplitude approximation

$$(M_x, M_z) = M(\sin\theta, \cos\theta), \quad (3.11)$$

$$(N_x, N_z) = N(\sin\phi, \cos\phi), \quad (3.12)$$

with M and N treated as constant. This describes the

reconstruction in terms of constant-magnitude vectors \mathbf{M} and \mathbf{N} rotating through angles θ and ϕ from the z axis. The approximation should be a good one at low temperatures, but it cannot be valid at temperatures that are too close to the critical temperature of gadolinium. To be more specific, the constant-amplitude approximation should be reasonable if the variation in the magnitude of the spin is small, say no more than 20% between the maximum and minimum values. In the microscopic model we found that the largest variation in spin magnitudes occurred in the Gd films, with the Gd spins near the interfaces having the largest magnitude (close to the $T=0$ value) and those in the center having the smallest value (close to that for spins in bulk Gd at the particular temperature under consideration). The decrease in the spin magnitude from the edge of the Gd film to the center was steady and showed no oscillations. Thus the ratio S_{\min}/S_{\max} is approximately given by $S(T)/S(0)$. For Gd, $S(T)/S(0)=0.8$ at a temperature of about $0.68T_c$, about 200 K. Thus one would expect the constant-amplitude approximation to be reasonable for the range 0–200 K.

The functional dependence of the free energy F on θ and ϕ is

$$\begin{aligned} \frac{F}{A} = & \int_{-d_1}^0 dy \left[-B_0 M \cos\theta + \frac{1}{2} c_1 M^2 \left(\frac{d\theta}{dy} \right)^2 \right] + \int_0^{d_2} dy \left[-B_0 N \cos\phi + \frac{1}{2} c_2 N^2 \left(\frac{d\phi}{dy} \right)^2 \right] \\ & + \alpha MN \cos(\theta - \phi) \Big|_{y=0} + \alpha MN \cos(\theta - \phi) \Big|_{y=-d_1}, \end{aligned} \quad (3.13)$$

where A is the specimen area in the x - z plane. The equations for minimum F are

$$c_1 M^2 \frac{d^2 \theta}{dy^2} - B_0 M \sin\theta = 0, \quad (3.14)$$

$$c_2 N^2 \frac{d^2 \phi}{dy^2} - B_0 N \sin\phi = 0, \quad (3.15)$$

with boundary conditions at $y=0$

$$c_1 M^2 \frac{d\theta}{dy} - \alpha MN \sin(\theta - \phi) = 0, \quad (3.16)$$

$$c_2 N^2 \frac{d\phi}{dy} - \alpha MN \sin(\theta - \phi) = 0. \quad (3.17)$$

Equations (3.14) and (3.15) describe “upside-down” pendula; the reason why they are upside down is explained by Ribeiro Filho *et al.*¹³ The first integral of (3.14) is

$$\frac{1}{2} \left(\frac{d\theta}{dy} \right)^2 + \lambda_1^2 \cos\theta = l_1^2, \quad (3.18)$$

where

$$\lambda_1^2 = B_0 / c_1 M \quad (3.19)$$

and l_1^2 is the constant of integration. One can obtain a similar first integral for Eq. (3.15) with a $\lambda_2^2 = B_0 / c_2 N$ as the integration constant.

The remainder of this section is devoted to solutions of (3.14)–(3.18). Appropriate numerical values of the various numerical parameters are given in Appendix A.

C. Semi-infinite media

We start with the relatively simple case of two semi-infinite media in contact, d_1 and $d_2 \rightarrow \infty$. For any nonzero value of B_0 , the spins are aligned with \mathbf{B}_0 at a large distance from the interface. Thus $\theta \rightarrow 0$ and $d\theta/dy \rightarrow 0$ as $y \rightarrow -\infty$, with the result that the constant of integration in (3.18) is

$$l_1^2 = \lambda_1^2. \quad (3.20)$$

Equation (3.14) is now solvable in terms of hyperbolic functions; in fact

$$\cos \frac{1}{2} \theta = \tanh[\lambda_1(y_1 - y)], \quad (3.21)$$

and similarly

$$\cos \frac{1}{2} \phi = \tanh[\lambda_2(y - y_2)], \quad (3.22)$$

where y_1 and y_2 are constants of integration. In the twisted state, both \mathbf{M} and \mathbf{N} turn away from the z axis; the signs of θ and ϕ are chosen, arbitrarily, so that $\theta > 0$ and $\phi < 0$. Note that $y < 0$ in (3.21) and $y > 0$ in (3.22). The solutions we find always have $y_1 > 0$ and $y_2 < 0$, so that θ and ϕ lie within the ranges $0 \leq \theta < \pi$ and $-\pi < \phi \leq 0$.

Given these solutions, it is easy to evaluate F/A from (3.13):

$$F - F_A = (4B_0M/\lambda_1)(1-t_1) + (4B_0N/\lambda_2)(1-t_2) + \alpha MN[(2t_1^2-1)(2t_2^2-1) - 4t_1t_2(1-t_1^2)^{1/2}(1-t_2^2)^{1/2}], \quad (3.23)$$

where

$$t_1 = \tanh(\lambda_1 y_1), \quad (3.24)$$

$$t_2 = \tanh(-\lambda_2 y_2), \quad (3.25)$$

and F_A is the free energy of the (spurious) fully aligned state with $\theta = \phi = 0$ and $\alpha = 0$. Minimization of $F - F_A$ with respect to t_1 and t_2 now yields values of the constants of integration y_1 and y_2 , and the angles θ and ϕ are found from (3.21) and (3.22).

Examples of reconstruction predicted in this way are shown in Fig. 9. As in previous calculations⁷ based on the mean-field theory of Sec. II, and as expected on general grounds, the width of the reconstructed region decreases as the applied field B_0 increases. Note that the length scale used in Fig. 9 is large compared with interatomic spacing, so that the reconstruction is spread over a substantial number of atomic planes.

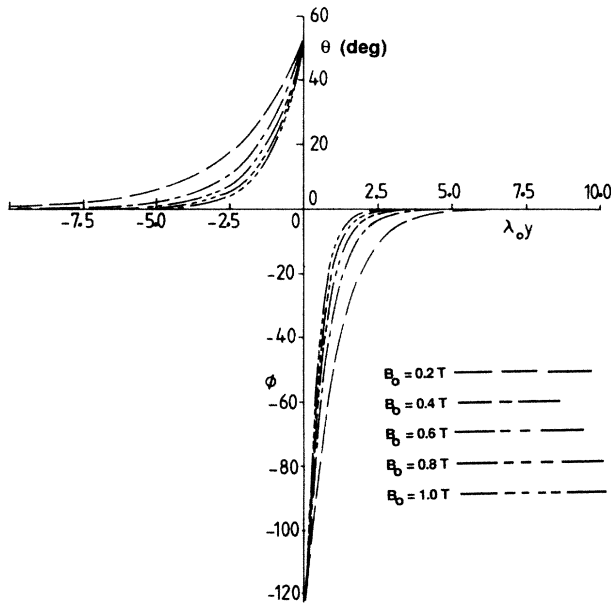


FIG. 9. Variation of θ and ϕ with position y (measured in m) for a single interface between iron and gadolinium. λ_0 has the value $5.85 \times 10^7 \text{ m}^{-1}$. For higher magnetic fields, the variation in angle takes place over a narrower region.

D. Superlattice reconstruction

We now turn to superlattices, in which d_1 and d_2 in Fig. 1 are finite. As discussed in Sec. II, the superlattice reconstruction is periodic, so that $\theta(y+L) = \theta(y)$ and $\phi(y+L) = \phi(y)$, where $L = d_1 + d_2$ is the superlattice period. Furthermore, in the unit cell, θ is symmetric about $y = -d_1/2$ and is symmetric about $y = d_2/2$.

Within the constant-amplitude approximation, (3.14)–(3.18) continue to apply. Now, however, the equations must be solved for general values of the constants of integration l_1^2 and l_2^2 . Since $d\theta/dy = 0$ at $y = -d_1/2$ and $d\phi/dy = 0$ at $y = d_2/2$, it is seen from (3.18) and the corresponding equation for ϕ that

$$0 < l_i^2 < \lambda_i^2, \quad i = 1, 2. \quad (3.26)$$

The solution of (3.18) can be given in terms of elliptic functions; the forms that satisfy the symmetry requirements on θ and ϕ are

$$\cos(\frac{1}{2}\theta) = -m_1^{1/2} \text{sn}(\lambda_1(y + \frac{1}{2}d_1) - K_1 | m_1), \quad (3.27)$$

$$\sin(\frac{1}{2}\theta) = \text{dn}(\lambda_1(y + \frac{1}{2}d_1) - K_1 | m_1), \quad (3.28)$$

$$\cos(\frac{1}{2}\phi) = m_2^{1/2} \text{sn}(\lambda_2(y - \frac{1}{2}d_2) + K_2 | m_2), \quad (3.29)$$

$$\sin(\frac{1}{2}\phi) = -\text{dn}(\lambda_2(y - \frac{1}{2}d_2) + K_2 | m_2), \quad (3.30)$$

where

$$m_i = (l_i^2 + \lambda_i^2)/2\lambda_i^2, \quad K_i = K(m_i), \quad i = 1, 2. \quad (3.31)$$

The signs have been chosen so that $\theta > 0$ and $\phi < 0$.

The expression for the free energy F can be evaluated

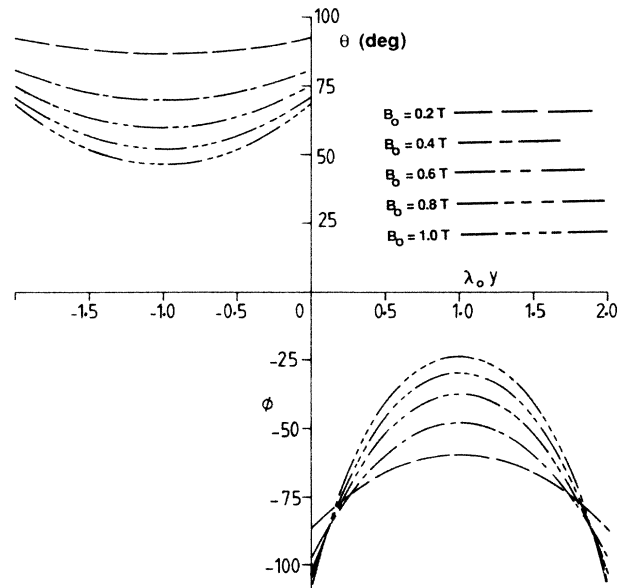


FIG. 10. Equilibrium configurations for an Fe-Gd superlattice with $d_1 = d_2 = 2\lambda_0^{-1}$ for different values of an applied field. λ_0 has the value $5.85 \times 10^7 \text{ m}^{-1}$. Note the similarity to the microscopic results presented in Fig. 5.

from these forms, and the result is given in Appendix B. In order to find the equilibrium configuration, we minimize F with respect to variations of the constants of integration l_1^2 , and l_2^2 within the domains given by Eq. (3.26). In practice, it is somewhat easier to minimize with respect to m_1 and m_2 , both lying within $0 < m < 1$, as seen from (3.31).

An example of reconstruction in a superlattice as derived from the above results is shown in Fig. 10. For the thicknesses used in that figure, the interface energy plays a very important part, and the reconstruction ensures that $\theta - \phi \approx 180^\circ$ for spins near the interface for all values of applied field B_0 . As is to be expected, the angles change more rapidly in larger fields.

IV. SUMMARY

We have investigated the equilibrium structure of a magnetic superlattice formed from two ferromagnetic materials which couple antiferromagnetically at the interfaces. We first studied superlattices using a microscopic approach. In contrast to a superlattice with ferromagnetic films which couple ferromagnetically, a variety of phases can exist in this system. There are two aligned phases, aligned-Fe and aligned-Gd, where all the spins are either parallel or antiparallel to an applied field. In addition there is a twisted phase where the spins in each layer lie at some angle with respect to the applied field. The phase diagram, and thus macroscopic quantities such as ir absorption or magnetic susceptibility, is a sensitive function of layering pattern. Changes of a few atomic layers in a film can have very dramatic effects on the phase diagram.

Some macroscopic applications may involve fairly thick films. In this case it is appropriate to use a macroscopic Landau-Ginzburg approach. Two geometries were discussed in detail: (1) two semi-infinite ferromagnets which are antiferromagnetically coupled at the interface; and (2) the superlattice structure with ferromagnetic films which are antiferromagnetically coupled. Here we studied the structure of the twisted phase at $T=0$ and presented analytic expression for the twist angle as a function of position.

Clearly a number of extensions to this work are appropriate. More realistic calculations would include anisotropy energies. Furthermore the influence of the interface exchange parameter has not been completely explored. Finally, in a finite superlattice there might be surface phase transitions which we have not discussed here.

ACKNOWLEDGMENTS

The authors are grateful for support from the United Kingdom Science and Engineering Research Council and from the U.S. Army Research Office under Grant No. DAAG29-84-K-0201.

APPENDIX A: NUMERICAL ESTIMATES

Appropriate expressions for estimating numerical values are given by Kittel,¹⁴ and the values used here for

TABLE I. Numerical values for Fe and Gd.

	T_c (K)	M (A m ⁻¹)	J (J)	C (SI)
Fe	1043	1.385×10^5	3.087×10^{-22}	2.110×10^{-21}
Gd	293	1.600×10^5	4.042×10^{-23}	2.424×10^{-22}

Fe and Gd are given in Table I. Exchange constants are evaluated from the standard expression

$$J = 3k_B T_c / 2zS(S+1)$$

and estimates of c are taken from

$$c = 6J / d\beta^2,$$

where β is the numerical value of M/S . For the interface exchange constant we assume $J_I = J_{Fe}$, as was done by Camley;¹¹ this gives

$$\alpha = 7.453 \times 10^{-13} \text{ SI}.$$

In numerical work, lengths are scaled in terms of λ_B^{-1} , where

$$\lambda_B = (c_1 M)^{-1/2} = 5.850 \times 10^7 \text{ m}^{-1} \text{ T}^{-1/2}.$$

The parameters λ_1 and λ_2 of Eq. (3.18) and its analogue are

$$\lambda_1 = B_0^{1/2} \lambda_B,$$

$$\lambda_2 = 2.310 B_0^{1/2} \lambda_B.$$

Numerical values are presented in Table I.

APPENDIX B: FREE-ENERGY EXPRESSION FOR A SUPERLATTICE

The expression for the free energy is found by substitution of the solutions (3.27)–(3.30) into (3.13). The two interface terms are equal because of the symmetry of θ and ϕ about the midpoints $y = -\frac{1}{2}d_1$ and $y = \frac{1}{2}d_2$. The integrals occurring can all be evaluated explicitly, and the final expression for the free energy is

$$F = F_{11} + F_{12} + F_{21} + F_{22} + F_I, \quad (\text{B1})$$

where

$$F_{11} = (2B_0 M / \lambda_1) [E(K_1 | m_1) - E(K_1 - \frac{1}{2}\lambda_1 d_1 | m_1)],$$

$$F_{12} = 2c_1 M^2 \lambda_1 m_1 [E(K_1 | m_1) - E(K_1 - \frac{1}{2}\lambda_1 d_1 | m_1) \quad (\text{B2})$$

$$- \frac{1}{2}(1 - m_1)\lambda_1 d_1], \quad (\text{B3})$$

$$F_{21} = (2B_0 N / \lambda_2) [E(K_2 | m_2) - E(K_2 - \frac{1}{2}\lambda_2 d_2 | m_2)], \quad (\text{B4})$$

$$F_{22} = 2c_2 N^2 \lambda_2 m_2 [E(K_2 | m_2) - E(K_2 - \frac{1}{2}\lambda_2 d_2 | m_2) \quad (\text{B5})$$

$$- \frac{1}{2}(1 - m_2)\lambda_2 d_2],$$

$$F_I = 2\alpha MN [(m_1 \text{sn}_1^2 - \text{dn}_1^2)(m_2 \text{sn}_2^2 - \text{dn}_2^2) \quad (\text{B6})$$

$$+ 4(m_1 m_2)^{1/2} \text{sn}_1 \text{dn}_1 \text{sn}_2 \text{dn}_2],$$

and

$$m_i = (l_i^2 + \lambda_i^2) / 2\lambda_i^2, \quad K_i = K(m_i), \quad i = 1, 2, \quad (\text{B7})$$

$$\begin{aligned} \text{sn}_1 &= \text{sn}(\frac{1}{2}\lambda_1 d_1 - K_1 | m_1) \\ \text{dn}_1 &= \text{dn}(\frac{1}{2}\lambda_1 d_1 - K_1 | m_1), \end{aligned} \quad (\text{B8})$$

$$\begin{aligned} \text{sn}_2 &= \text{sn}(-\frac{1}{2}\lambda_2 d_2 + K_2 | m_2) \\ \text{dn}_2 &= \text{dn}(-\frac{1}{2}\lambda_2 d_2 + K_2 | m_2). \end{aligned} \quad (\text{B9})$$

K is the complete elliptic integral of the second kind, and E is the incomplete elliptic integral. All notation is the same as in Abramowitz and Stegun.¹⁵

¹L. L. Hinchey and D. L. Mills, Phys. Rev. B **33**, 3329 (1986).

²L. L. Hinchey and D. L. Mills, Phys. Rev. B **34**, 1689 (1986).

³F. Fishman, F. Schwabl, and D. Schwenk, Phys. Lett. A **121**, 192 (1987).

⁴M. Taborrelli, R. Allenspach, G. Boffa, and M. Landolt, Phys. Rev. Lett. **56**, 2869 (1986).

⁵D. Weller, S. F. Alvarado, W. Gudat, K. Schroder, and M. Campagna, Phys. Rev. Lett. **54**, 1555 (1985).

⁶P. Grünberg, R. Schreiber, Y. Pang, M. B. Brodsky, and H. Sowers, Phys. Rev. Lett. **57**, 2442 (1987).

⁷C. Carbone and S. F. Alvarado, Phys. Rev. B **36**, 2433 (1987).

⁸J. Krebs, C. Vittoria, B. T. Jonker, and G. A. Prinz, J. Magn.

Magn. Mater. **54-57**, 811 (1986).

⁹P. X. Zhang and W. Zinn, Phys. Rev. B **35**, 5219 (1987).

¹⁰J. W. Cable and W. C. Koehler, J. Appl. Phys. **53**, 1904 (1982).

¹¹R. E. Camley, Phys. Rev. B **35**, 3608 (1987).

¹²M. G. Cottam, D. R. Tilley, and B. Zeks, J. Phys. C **17**, 1793 (1984).

¹³A. Riberio Filho, D. R. Tilley, and B. Zeks, Phys. Lett. **100A**, 247 (1984).

¹⁴C. Kittel, *Introduction to Solid State Physics* (Wiley, New York, 1986).

¹⁵*Handbook of Mathematical Functions*, edited by M. Abramowitz and I. Stegun (Dover, New York, 1972).